Journal of Physical Oceanography

The DOI for this manuscript is doi: 10.1175/2009JPO4106.1

Amplification of a Surface-intensified Eddy Drift along Steep Shelf in the Eastern Mediterranean Sea

Georgi Sutyrin [1]

Graduate School of Oceanography, University of Rhode Island, Narragansett, RI 02882, USA

Alexander Stegner

Laboratoire de Meteorologie Dynamique, Centre National de la Recherche Scientifique (CNRS), Ecole Normale Superieure (ENS), 24 Rue Lhomond, 75005 Paris, France

Isabelle Taupier-Letage and Samuel Teinturier

Universite de la Mediterranee, Centre National de la Recherche Scientifique (CNRS UMR 6535), Centre d'Oceanologie de Marseille, Antenne de Toulon, BP 330, 83507 La Seyne, France

[1] *Corresponding author address:* Georgi Sutyrin, Graduate School of Oceanography, University of Rhode Island, Narragansett, RI 02882, USA.
E-mail: gsutyrin@gso.uri.edu

ABSTRACT

The data sets of the EGYPT(Eddies and GYres Paths Tracking)/EGITTO program in the eastern Mediterranean sea reveal a large mesoscale anticyclone traveling along the Libyan shelf. Surface drifters trajectories combined with a CTD transect quantify accurately the horizontal velocity and the vertical structure of this surface-intensified anticyclone. The observed westward drift speed is significantly higher than expected from the beta-effect only. In order to study the impact of a steep shelf topography on the propagation of compact, surface-intensified vortices, we used a two-layer beta-plane model with steep continental slope and nearly zonal boundary. A perturbation theory derived by Sutyrin (2001) for a circular vortex in the upper layer with the lower layer at rest as a basic state is generalized for non-uniform slope in the presence of the image-effect. An integral momentum balance is used to derive the drifting velocity of an upper layer vortex with the main assumption that a stable and a steady drifting solution of the two layer system exists. The interface is described by a steady drifting circular dome at the leading order. This approach allows to reduce the problem to the calculation of the deep-flow pattern, depending on the interface shape and topography. When the topographic slope beneath the eddy changes rapidly from a steep continental slope to a gentle continental rise, most part of the deep-flow pattern is shifted offshore. The corresponding anticyclonic deep-flow feedback provides an additional along-slope propagation, which is proportional to the basic drift speed and the steepness parameter.

Keywords: mesoscale anticyclone, vortex drift, stratification, steep shelf, Mediterranean sea.

1 Introduction

Surface-intensified baroclinic eddies are often affected by continental slopes. Recent observations of the EGYPT(Eddies and GYres Paths Tracking)/EGITTO program quantify the horizontal and the vertical structure of a surface anticyclonic eddy drifting along the Libyan shelf. However, understanding of the leading dynamical processes in interaction of large-scale eddies with steep topography is limited. The aim of this paper is to clarify dominant physical mechanisms which are crucial for modeling eddy evolution in the presence of steep bathymetry and horizontal boundaries. We focus this study on surface-intensified eddies interacting with topography of limited lateral extent (e.g. continental slopes with steep gradients), as opposed to slowly varying topography which has been the subject of some recent developments.

1.1. Background

Eddies or rings of the western boundary currents are amongst the most intense oceanic localized structure and there is much observational evidence that they are typically transformed encountering continental slopes and shelves. Examples were described for Gulf Stream rings (Evans et al. 1985; Brown et al. 1986), Loop Current rings in the Gulf of Mexico (Kirwan et al. 1988; Vukovich and Waddell 1991), North Brazil Current rings (Fratantoni et al. 1995), North Pacific eddies (Umatani and Yamagata 1987), East Australian Current rings (Hamon 1965; Freeland et al. 1986), etc. These observations do not easily lend themselves to a canonical description of either the interaction processes or its results. Theses rings or eddies may remain near the shelf break or move offshore (Puillat *et al.* 2002) and there may be significant modification of the shelf water mass. In particular, our observations of eddy evolution in the vicinity of nearly zonal boundaries indicate along-slope drift essentially faster than expected from the beta-effect only (Fig. 1).

This variability of eddy interactions with continental slope and shelves indicates that there should be a number of variables that govern these interactions, and a number of authors have contributed theoretical insight likely to be relevant in explaining the behaviors observed. Some of the earliest studies of vortex-topography interaction have used a depth-averaged barotropic model (e.g., Firing and Beardsley (1976), Louis and Smith (1982) and Grimshaw et al. (1994) demonstrated the rapid dispersion into topographic Rossby waves of eddies over a steep continental slope). Reorganization of the barotropic vortex structure due to various topographic effects was considered in a number of laboratory, numerical and theoretical studies (e.g., Carnevale et al. 1991; Wang 1992; van Heijst 1994; McDonald 1998; van Geffen and Davies 1999; Richardson 2000).

The real ocean is stratified and baroclinic rings are typically surface-intensified, so that their main core is not in direct contact with the topography. The deep-flow feedbacks on their evolution were often modeled using two-layer models with topographic slope represented by a variable depth in the lower layer (e.g., Smith and O'Brien, 1983; Smith, 1986; Kamenkovitch et al, 1996, Thierry and Morel, 1999; Reznik and Sutyrin, 2001; Sutyrin, 2001, Jacobs et al., 2002; Kizner et al., 2003; Sutyrin et al., 2003; Sutyrin and Grimshaw, 2005)

In contrast with the above studies focused on the deep-flow topographic feedback, the dynamics of eddies interacting with boundaries have been analyzed in the reduced-gravity setting with a vertical wall (e.g., Nof 1999 and the references therein). The interaction of a lens-like anticyclone with a vertical wall involves a competition between at least three processes: the so-called image effect, which produces a poleward migration of anticyclones; a β-induced equatorward drift that becomes pronounced when the eddy encounters the western boundary; and a poleward propagation due to ejection of mass equatorward from the eddy. In the context of reduced-gravity

lens-like eddy, these processes are essentially in balance, and the eddy slowly decays as it moves into the wall without substantial meridional migration.

Recent numerical experiments by Frolov et al. (2004) included a more realistic continental shelf that is allowed to penetrate all the way into the upper layer, when isopycnals intersect bathymetry. The physical mechanism that has the most significant effect on the evolution of the anticyclonic vortex is shown to be a vortex-induced water exchange between shallow shelf with high potential vorticity and upper layer water at the vortex periphery with low potential vorticity over the deep ocean. The vortex interaction with secondary upper layer cyclones that are generated by off-shelf advection of high potential vorticity results in the vortex becoming elliptic and rotating clockwise with its center following a cycloidal trajectory with a net southward drift. The characteristic pattern of vortex evolution seen in the numerical experiments can be identified in some observed cases of Loop Current Eddy interaction with the western boundary in the Gulf of Mexico.

Abrupt topography penetrating all the way into the upper layer can be considered within quasigeostrophic models where the height of topography in the upper layer is small in comparison with the mean depth of the upper layer (e.g., Thompson 1993; Dewar and Leonov 2004; White and McDonald 2004). Dynamics of waves and vortices in the vicinity of finite step-like topography with two-layer fluid on one side of the step and just one layer on the other side were shown to be significantly different than that of more conventional models with topography occupying a small fraction of the depth of the lower layer.

Evaluation of deep-flow topographic feedback on the evolution of surface-intensified eddies is a difficult and fundamental problem; there is presently very limited understanding of its implications. A number of the previous studies of topographic effects on eddies have been summarized by Sutyrin (2001) and by Jacob *et al.* (2002). An

inviscid asymptotic theory was proposed by Sutyrin (2001) that allows for the description of the deep-flow pattern beneath a surface-intensified vortex on the β-plane over a steep topographic slope, and the subsequent estimation of its feedback on the vortex drift for an arbitrary slope orientation. However, the theory was developed for uniform and weakly non-uniform slope that is not able to describe the deep-flow in the presence of strongly non-uniform slope.

1.2. This paper

The detailed sampling of an anticyclonic eddy off Libya provides strong observational basis for eddy-slope interactions. Here we focus on the baroclinic eddy evolution near a steep continental slope and gentle continental rise using asymptotic analysis in the two-layer setup generalizing the theory by Sutyrin (2001).

The rest of the paper is organized as follows. The horizontal and vertical structures of the meso scale anticyclone drifting along the Libyan shelf are given in section 2. The two-layer dimensionless model and the perturbation theory are formulated in section 3. In section 4 the lower-layer flow pattern and the corresponding deep-flow feedback are evaluated for a combination of steep and gentle slopes. Numerical modeling is described in section 5. The discussion and conclusions are presented in section 6.

2 Structure and trajectory of a meso scale anticyclone along the Libyan shelf.

The EGYPT-1 campaign took place in April 2006. The infrared satellite imagery was analysed in near real time to retrieve information on the mesoscale structures. It enabled sampling along the Libyan shelf of a meso scale anticyclone (hereafter called Libyan Eddy: LE) with a CTD transect (figure.1(d)) and with surface drifters (see http://poseidon.ogs.trieste.it/sire/drifter/egitto_0406_sem.html). Among them, three drifters remain trapped in the core of the *LE anticyclone* for several months.

Unlike the usual eddies generated by the instability of the Libyo-Egyptian current that drift eastward (Hamad *et al.* 2005, Millot and Taupier-Letage, 2005), both the drifters and the infrared satellite images showed that the LE anticyclone drifted westward for more than one year (Taupier-Letage, 2008). The analysis of these in-situ observation is presented below.

2.1 Surface drifters and eddy trajectories

The trajectories of the three surface drifters (released between April 10 and 11, 2006) that remained trapped in the *LE anticyclone* are shown in the figure 1. The ARGOS positioning system provides their latitude and longitude with a high temporal frequency. The Kriging method (Poulain and Zambianchi, 2007) was used to filter the data set and extract the position (X_i, Y_i) and the instantaneous speed vector $\underline{V}_i$ of the drifters every six hours. One buoy nB57312 remain trapped in the core of the *LE anticyclone* from April to September (figure 1a), while the other two (nB59774 and nB59777) remained trapped from April to July (figure 1(b) and 1(c)). The drifters loop inside the eddy with approximately the same mean period of five days. Hence, when we filter out these rapid oscillations on both the latitude and the longitude data set for the three drifters, we can extract the slow evolution of the eddy center. The trajectory of the *LE anticyclone* is then interpolated. The westward drift of the *LE anticyclone*, following the Libyan shelf, is shown in figure 1d. Surprisingly, the distance between the vortex center and the $-200m$ bathymetry remain almost constant $L \sim 55 - 65km$. The *LE anticyclone* propagates westward, along a steep shelf bathymetry, with a mean speed of $V_{LE} \simeq 1 - 2km/day$.

2.2 The core rotation of the *LE anticyclone*

Using the eddy trajectory plotted in figure 1(d), we could calculate for each successive position (X_i, Y_i) the radial distance R_i from the drifter to the eddy center.

We plot in the figure 2 the couple of data (R_i, V_i) measured every six hours during the 5-month period (April to September) when the drifter nB57312 remained trapped inside the eddy (figure 1(a)). The intermittency of the local wind stresses or the small scale waves activity induce a dispersion in the drifters dynamics and a wide range of R_i values are explored while the drifters loop inside the eddy. We could, in a first approximation, assume a steady solid body rotation of the vortex core during this 5-month period and fit these data with a linear relation $V_i = \Lambda R_i$. According to the figure 2 we get an angular rotation rate $\Lambda \simeq 10^{-5} rad.s^{-1}$ and the maximum velocity seems to be reached for $R \simeq 30 - 35km$. The core vorticity $\zeta_{LE} = 2\Lambda \simeq 2\,10^{-5} rad.s^{-1} \simeq 0.25\, f_0$ remains moderate in comparison with the local Coriolis parameter $f_0 = 7.8\,10^{-5} rad.s^{-1}$.

2.3 The vertical structure of the *LE anticyclone*

The thirty CTD profiles were taken between April 19 and 21, 2006. We plot in figure 1(d) the locations of these CTD profiles and the estimated position of the vortex center at that time according to the drifters trajectories analysis 2.1. A $35km$ circle indicates the radius of maximum velocity or, in other words, the core of the *LE anticyclone*. This CTD transect crosses the eddy close to its center. The horizontal sampling of this transect is about $10km$ while the vertical resolution is close to $1m$. We extracted, from these high resolution measurements, a typical density cross section of the vortex figure 3(a). The unperturbed thermocline depth is about $150m$ while in the vicinity of the vortex center it could reaches $300m$. Hence, the relative isopycnal deviation induced by the *LE anticyclone* is finite. For a geostrophically balanced vortex, such a large isopycnal deviation could only be induced by an eddy which is large enough in comparison with the deformation radius R_d of the first baroclinic mode. Indeed, if we estimate this latter, according to the vertical stratification outside

the anticyclone, we get $R_d \simeq 13km$ which is significantly smaller than the core vortex size $R \simeq 30 - 35km$. Moreover, we add on figure 3(a) the seafloor bathymetry along the transect. The center of this surface-intensified eddy seems to be located above the breaking point of the shelf topography figure 3(a). The slope of the sea shelf is about $p = 10\%$ which is much steeper than the isopycnal slope ($\sim 0.5\%$) in the anticyclonic vortex figure 3(b). Hence, the *LE anticyclone* drifts along a steep shelf topography.

2.4 Dimensional analysis

According to theses in-situ measurements we could quantify accurately the various dynamical parameters which control the dynamics and the eddy trajectory. Both the standard Rossby number $Ro = V_0/fL \simeq 0.12$ or the dynamical Rossby number $\varepsilon = \zeta_{LE}/f \simeq 0.25$ are small, where V_0 is the maximum eddy velocity, R is the characteristic radius and ζ_{LE} is the core vorticity. Hence, the *LE anticyclone* satisfy the geostrophic balance at the first order of approximation. Besides, the typical eddy radius R is significantly larger than the local dformation radius $R_d \simeq 13km$ leading to a small Burger number $Bu = (R_d/R)^2 \simeq 0.16$. The Burger number of a coherent vortex is directly proportional to the kinetic to potential energy ratio and therefore, the potential energy stored in the vortex remain large in comparison with its kinetic energy. We also introduce $\delta = h_0/H_0$ the aspect ratio of the upper thermocline thickness $h_0 \simeq 150m$ to the depth H_0 of the barotropic lower layer. For a two-layer system, the layer thickness ratio δ controls the dynamical interactions between the two layers. The growth rate of baroclinic unstable modes, if any, are strongly reduced for small values of δ. Besides, according to Cushman-Roisin et al. (1992) the upper layer is not affected, at the first order of approximation, by the lower dynamics when $\delta \ll min(1,\, Bu^2)$. However, even if the layer thickness ratio $\delta \simeq 0.08$ is small this value is not negligible in comparison with the square of the Burger

number $Bu^2 \simeq 0.02 - 0.03$. Hence, the lower layer motion may nevertheless play a significant role in the upper layer dynamics as demonstrated below. The parameter C quantifies the amplitude of the vortex drift V_{LE} in comparison with the maximum eddy velocity V_0. In other words, C is related to the slow evolution of the vortex in comparison with the eddy turnover time. According to the small value of $C \simeq 0.04$, the *LE anticyclone* evolve slowly and is expected to have closed streamlines and to trapped a large amount of water in its core. The last parameter To measure the relative amplitude of the shelf slope in comparison with the isopycnal slopes induced by the geostrophic motion of the surface intensified vortex.

All these dynamical parameters are summarized in the Table below.

As far as the westward drift speed of a mesoscale vortex is concerned, we should estimate the maximum phase speed of Rossby waves associated to the first baroclinic mode. According to the local deformation radius $R_d \simeq 13km$, this phase speed is about $V_\beta = \beta R_d^2 \simeq 0.2km/day$. If we consider the westward drift of an isolated anticyclone in a reduced gravity shallow-water model (Nezlin and Sutyrin, 1994; Stegner and Zeitlin, 1995, 1996) nonlinear effects induced by the finite isopycnal deviation may lead to a supercritical drift speed of $V_d \simeq V_\beta(1 + a\lambda)$ where a is a geometrical factor which depends on the eddy shape. If we take $a \simeq 1$ in first approximation we get $V_d \simeq 0.4km/day$. Hence, if we do not take into account the bottom topography or the influence of the coastline, the nonlinear beta drift underestimate the measured drift velocity $V_{LE} \simeq 1.3 - 2km/day$ of the *LE anticyclone*.

3 A two-layer model

3.1 Two-Layer Equations

We consider a two-layer, rotating fluid in the Boussinesq, hydrostatic, rigid-lid, and β-plane approximations along a steep shelf topography (Fig. 4). The layer densities

are ρ_j, the depths are h_j, the pressure field is p_j, and the velocity vector is $\mathbf{v}_j = (u_j, v_j)$, where $j = 1$ and $j = 2$ represent variables in the upper and the lower layer, respectively.

First, we non-dimensionalize the variables as follows:

$$(\hat{X}, \hat{Y}) = (X, Y)/R, \qquad \hat{t} = tV_0/R, \qquad \hat{f} = f/f_0, \tag{1}$$

$$(\hat{u}_j, \hat{v}_j) = (u_j, v_j)/V_0, \quad \hat{h}_1 = h_1/h_0, \quad \hat{h}_2 = h_2/H_0, \quad \hat{H}_T = H_T(y)/H_0, \qquad \hat{p}_j = p_j/\rho_j g' h_0 \tag{2}$$

where R and $V_0 = Ro\, f_0 R$ are respectively the eddy radius and the characteristic eddy velocity, h_0 is the mean upper layer depth, $g' = (\rho_2 - \rho_1)g/\rho_1$ is the reduced gravity, and f_0 is the Coriolis parameter at the reference latitude. We introduce here the standard horizontal scale $R_d = \sqrt{g'h}_0/f_0$ which corresponds to the baroclinic deformation radius when $\delta = h_0/H_0 \ll 1$ and $\rho_2 - \rho_1 \ll \rho_1$. Finite interface deviation could occurs under geostrophic balance when $Bu = (R_d/R)^2 \ll 1$ (such as the *LE anticyclone* or cyclogeostrophic balance when $Ro = (R_d/R)^2 \simeq 1$. Hence, in this section we do not make any assumptions on the Rossby number Ro or the two-layer aspect ratio δ and the calculation remain valid if theses parameters are equal to unity.

After the hats for the non-dimensional variables are dropped, the momentum and continuity equations become

$$Ro\,[\partial_t \mathbf{v}_j + (\mathbf{v}_j \cdot \nabla)\mathbf{v}_j] + f\mathbf{k} \times \mathbf{v}_j = -\nabla p_j, \tag{3}$$

$$\partial_t h_j + \nabla \cdot (h_j \mathbf{v}_j) = 0, \qquad h_2 = H_T(Y) + \delta(1 - h_1) \tag{4}$$

where ∇ is the horizontal gradient operator, and $\mathbf{k}$ is the vertical unit vector. The pressure and upper layer thickness gradients are related by the hydrostatic equation:

$$\nabla h_1 = \nabla(p_1 - p_2), \tag{5}$$

Both the horizontal dissipation and the bottom friction are neglected in this two-layer model. Hence, the potential vorticity q_j is conserved in fluid parcels for each layer:

$$(\partial_t + \mathbf{v}_j \cdot \nabla) q_j = 0, \qquad q_j \equiv \frac{f + Ro\, \mathbf{k} \cdot \nabla \times \mathbf{v}_j}{h_j}. \tag{6}$$

The right-hand coordinate system corresponds to the depth topography $H_T(Y)$, with the Y-axis directed offshore, and the X-axis parallel to the isobath. Thus, the dimensionless Coriolis parameter is $f = 1 + \beta Y$ and $\beta = f'R/f_0$ where f' is the dimensional northward gradient of the Coriolis parameter. Assuming a zonal boundary at $Y = -L$, where $L = L_c/R$ is the non-dimensional distance from the vortex center to the coast, we apply there the free slip boundary conditions $u_j = 0$.

Typically $\beta \simeq 10^{-2}$ and it is considered to have a small value here. A perturbation expansion in β was used by Sutyrin (2001) to construct a formula for the deep-flow feedback on the upper-layer vortex drift over weakly non-uniform sloping topography. Here, we use the similar methodology to consider the vortex drift along strongly non-uniform sloping topography taking into account also a weak image-effect and assuming a zonal boundary.

3.2 Perturbation Theory and the deep flow structure

When $\beta = 0$ (the f-plane) and $L = \infty$ (far from the wall), any circular vortex in the upper layer

$$p_1 = h_1 - 1 = P(r), \qquad \mathbf{V_1} = \Omega(r)(-Y, X), \qquad \frac{dP}{dr} = r\Omega(1 + \Omega) \tag{7}$$

with no motion in the lower layer ($\mathbf{v_2} = 0$) is a stationary solution of the two-layer system. The variables $P(r)$ and $\mathbf{V_1}(r)$, with $r = \sqrt{X^2 + Y^2}$, correspond here to the pressure and the velocity fields associated to this steady circular vortex. The presence of the image-effect and the β-effect induce a translation of the vortex center and could also disperse the initial structure (Firing and Beardsley, 1976; Masuda *et al.* 1990).

We assume here that a coherent and a steady drifting solution could be reached in the two-layer system. The characteristic drift speed due to the image effect and the β-effect are given respectively by $2L|\Omega(2L)| \ll 1$ and $V_\beta/V_0 = \beta\,(Bu/Ro) \ll 1$. In both cases, we consider a small drift speed in comparison with the characteristic eddy velocity, leading to a perturbation expansion in $C = V_d/V_0 \ll 1$. In such case, we assume that the circular vortex solution ($P(r)$ and $\mathbf{V_1}(r)$) will be slightly distorted by the weak β-effect, the wall effect and the lower layer bottom topography.

Therefore, we seek a stationary solution in the coordinate system ($x = X + Ct, y = Y$), translating along-slope with the velocity $(-C, 0)$. To satisfy the boundary condition, the image-effect is taken into account by adding the opposite sign vortex in the upper layer at the distance $y = -2L$ from the center of coordinates which generate additional flow of the order ε. For a sufficiently large distance from the coast, the velocity $\varepsilon\tilde{\mathbf{V}}$ and the pressure deviation $\varepsilon\tilde{P}$ induced by the image effect (at the vortex location) will be weak in comparison with the circular vortex flow.

$$\varepsilon\tilde{\mathbf{V}} = \Omega(\tilde{r})(y+2L, -x), \qquad \tilde{r}^2 = x^2 + (y+2L)^2, \qquad \varepsilon\frac{d\tilde{P}}{d\tilde{r}} = \tilde{r}\Omega(1-\Omega). \quad (8)$$

As mentioned before the drifting velocity of the anticyclone LE measured in the EGYPT campaign is small in comparison with the typical eddy velocity of the surface layer. Therefore, assuming $C \sim \varepsilon \ll 1$ leads to the following asymptotic expansion :

$$p_1 = P(r) - \varepsilon\tilde{P}(\tilde{r}) + C\eta + C\psi + O(C^2), \qquad h_1 = 1 + P(r) - \varepsilon\tilde{P}(\tilde{r}) + C\eta + O(C^2), \quad (9)$$

where p_1 is the upper layer pressure sum of the circular vortex pressure P, the pressure of the circular image vortex $\varepsilon\tilde{P}$, the interface deviation $C\eta$ induced by the steady translation and the lower layer pressure $C\psi$. We assume here that the steady drifting vortex structure trapped fluid parcels in the upper layer but not in the deep lower layer. In such case, the lower layer velocity V_2 cannot be larger than the drifting

velocity $V_d = CV_0$. Hence, we write for the velocity fields:

$$\mathbf{v_1} = \Omega(r)(-y, x) + \varepsilon\tilde{\mathbf{V}} + \mathbf{Cv} + O(C^2), \qquad \mathbf{v_2} = C\mathbf{k} \times \nabla\psi, \tag{10}$$

where v_1 is the upper layer velocity sum of the circular vortex velocity $\mathbf{V_1}(r)$, the image vortex velocity$\varepsilon\tilde{\mathbf{V}}$, the velocity contribution $\mathbf{Cv}$ due to the steady translation

$$p_2 = C\psi + O(C^2, \beta), \qquad h_2 = H_T(Y) - \delta P(r) + \delta\varepsilon\tilde{P}(\tilde{r}) - \delta C\eta + O(C^2). \tag{11}$$

The steadily translating perturbation given by (9)–(11) at leading order satisfies the following system, obtained by linearizing the original equations.

$$\mathbf{k} \times \mathbf{v} + \frac{\beta}{C} y\mathbf{k} \times \mathbf{V_1} + \nabla(\eta + \psi) = -Ro\left[\partial_x \mathbf{V_1} + ((\mathbf{v} + \tilde{\mathbf{V}}) \cdot \nabla)\mathbf{V_1} + (\mathbf{V_1} \cdot \nabla)(\mathbf{v} + \tilde{\mathbf{V}})\right] \tag{12}$$

$$\nabla \cdot ((1 + P)\mathbf{v} + \eta\mathbf{V_1}) = -\partial_x P + \frac{\varepsilon}{C}\nabla \cdot (\tilde{P}(\tilde{r})\mathbf{V_1} - (1+P)\tilde{\mathbf{V}}), \tag{13}$$

The upper-layer perturbations can be found in a manner similar to that proposed by Benilov (1996) in the reduced-gravity approximation with the lower layer at rest. However, the lower layer flows could be derived from the lagrangian conservation of the potential vorticity (6):

$$q_2 = \frac{1}{H_T(Y) - \delta P} + O(CRo, \beta) \tag{14}$$

$$D_t q_2^{-1} = J[C\psi - Cy, H_T(y) - \delta P(r)] + O(C^2 Ro, C\beta) = 0 \tag{15}$$

Hence, at the first order of approximation the deep flow structure depends only on the first order circular vortex solution $P(r)$ and the bathymetry $H_T(y)$. This implicit relation can then be easily integrated along characteristics to find an explicit expression for the lower layer flow pattern, but crucially, only when there are no closed contours of the lower layer streamfunction. In such case, we get

$$\psi = y - H_T^{-1}\left(H_T(y) - \delta P(r, t)\right) + O(CRo, \beta) \tag{16}$$

3.3 Integral constraints and the deep flow Feedback

As pointed out by Sutyrin (2001), it is not necessary to calculate the upper-layer perturbations in detail in order to find the propagation speed. Instead, it can be found from integral constraints in a manner similar to that proposed by Killworth (1983) and Nof (1983) assuming that the eddy is localized, i.e., the flow decays fast enough with r and all the following integrals are finite. First, multiplying the mass conservation equation (13) by x, and integrating by parts over the entire area, we obtain

$$M = -\int \left[(1+P)(u+\frac{\varepsilon}{C}\tilde{u}) + (\eta - \frac{\varepsilon}{C}\tilde{P}(\tilde{r}))U_1\right] dxdy = 2\pi \int Prdr = 2\pi \int (h_1 - 1)\, rdr, \tag{17}$$

where M is, at the first order of approximation, the mass excess of the upper layer vortex.

The momentum perturbation integral in (17) can be expressed using the momentum equation (12) multiplied by $1+P$ and integrated by parts over the entire area:

$$\int ((1+P)u + \eta U_1)dxdy = \frac{\beta}{C}\int (1+P)\Omega y^2 dxdy - \int (1+P)\partial_y \psi dxdy, \tag{18}$$

Here we use (9) to express the first integrals in the right-hand side by the sum of the mass excess M and the potential energyE_p

$$\int P\Omega x^2 dxdy = \int P\Omega y^2 dxdy = \pi \int P\frac{dP}{dr}r^2 dr = -E_p + O(Ro), \tag{19}$$

$$\int \Omega x^2 dxdy = \int \Omega y^2 dxdy = \pi \int \frac{dP}{dr}r^2 dr = -M + O(Ro) \tag{20}$$

where $E_p = \pi \int P^2 rdr$.

Finally we obtain at the first order of approximation:

$$C = \beta(1 + \frac{E_p}{M}) + \frac{\varepsilon}{M}\int \left(\tilde{P}(\tilde{r})U_1 - (1+P)\tilde{u}\right) dxdy + \frac{C}{M}\int (1+P)\partial_y \psi dxdy \tag{21}$$

The first term describes the β-drift in the reduced-gravity approximation found by Killworth (1983) and Nof (1983). The ratio E_p/M is positive for anticyclones and

negative for cyclones, and provides essential difference between evolution of cyclonic and anticyclonic eddies (e.g., Nezlin and Sutyrin, 1994). The second part describes the image-effect, while the third term describes an additional drift due to the lower layer flow feedback, which is the focus of this study.

From (21) we see that the evaluation of the topographic feedback on the vortex propagation consists of two steps. First, we have to obtain the solutions to (15) describing the components of the deep-flow pattern generated by the along-slope vortex drift depending on the interface shape. Second, inserting the solution for ψ into (21) allows us to calculate the drift velocity modified by the deep-flow feedback.

4 Deep-flow Feedback

In order to calculate the deep flow feedback on a surface intensified vortex, we choose here for simplicity an exponential shelf topography

$$H_T(Y) = 1 - \exp(-\delta To(y + L)) \qquad y \geq -L \tag{22}$$

This bottom slope is controlled by three parameters: the two layer aspect ratio δ, the topographic slope parameter To and the nondimensional distance from the vortex center to the coast L. According to the relation (16) we get the streamfunction in the coastal frame

$$\psi = \frac{1}{\delta To} \log\left(1 + \delta P(r) \exp(\delta To(y + L))\right) \tag{23}$$

This low-layer flow corresponds to an anticyclonic circulation with along-slope velocity

$$\frac{\partial \psi}{\partial y} = \frac{1}{To} \frac{\partial_y P + \delta To P}{\exp(-\delta To(y + L)) + \delta P} \tag{24}$$

The center of the deep-flow circulation is shifted offshore by the distance defined by $\partial_y P = -\delta To P$. We define the acceleration coefficient γ corresponding to the

additional drifting velocity due to the deep flow feedback according to (21)

$$C = (1+\gamma)\left[\beta(1+\frac{E_p}{M}) + \frac{\varepsilon}{M}\int\left(\tilde{P}(\tilde{r})U_1 - (1+P)\tilde{u}\right)dxdy\right] \tag{25}$$

a positive (negative) value of γ corresponds to an increase (decrease) of the steady drifting velocity induced by the deep layer bottom topography.

For an exponential shelf topography the acceleration coefficient γ satisfies (24)

$$\frac{\gamma}{1+\gamma} = \frac{1}{M}\int(1+P)\frac{\partial_y P + \delta To P}{To\left(\exp(-\delta To(y+L)) + \delta P\right)}dxdy. \tag{26}$$

This integral formula allows to estimate the acceleration coefficient depending on the circular vortex structure $P(r)$ and the parameters To and δ. In what follows we take a Gaussian upper layer vortex $P = \lambda\exp(-\frac{1}{2}r^2)$. For small aspect ratio parameter $\delta \ll 1$ we get, at the first order of approximation, in the lower layer a gaussian pressure field shifted offshore by the distance δTo

$$\psi = \frac{\lambda}{To}\exp(\delta To(L+\frac{1}{2}\delta To))\exp(-\frac{1}{2}(x^2+(y-\delta To)^2)) \tag{27}$$

Typical streamlines plotted in the steady drifting frame are shown in Figure 5 for both the upper and the lower layer. The surface intensified vortex trapped fluid within its core according to the closed streamlines of Fig. 5 (a) while the lower layer fluid parcels are simply deviated offshore Fig. 5 (b) without any fluid trapping. The acceleration coefficient γ is then given by the relation

$$\frac{\gamma}{1+\gamma} = \frac{\lambda}{M}\int_{-L}^{+\infty}(\delta To - y)\,dy\int_{-\infty}^{+\infty}dx\frac{\left(exp(-\frac{r^2}{2}) + \lambda exp(-r^2)\right)}{To\left(exp(-\delta To(y+L)) + \delta\lambda exp(-\frac{r^2}{2})\right)} \tag{28}$$

where $M = \lambda\sqrt{2\pi}\int_{-L}^{+\infty}exp(-y^2/2)\,dy$

We then study the variations of the acceleration coefficient γ according to the dimensionless parameters λ, δ and To. According to the Figure 6 (a) we have shown that for small values of the two-layer aspect ratio ($\delta \ll 1$) the drifting speed acceleration is mainly controlled by the product δTo. Hence, when $\delta To \simeq 2$ the deep

flow feedback induced by the steep shelf topography could increase the vortex drift by 100% or even more. When δTo becomes finite, the potential voricity gradient in the lower layer, due to the shelf slope, is of the same order of magnitude than the potential vorticity gradient induced by the upper layer vortex. In such case, the lower layer retroaction become significant and the acceleration coefficient increases strongly for steeper shelf slope. The relative amplitude of the isopycnal displacement λ, which is related to the relative size of the vortex in comparison with the local deformation radius, also control the acceleration coefficient (Figure 6 (b).

5 Numerical simulations

The previous integral relations (21) and (26) assume that a steady drifting vortex could be reached by the two-layer system. However, the existence and/or the stability of a coherent steady state cannot be guaranteed by the center of mass relation. Topographic Rossby or Kelvin wave radiations and or instabilities could strongly affect an initial vortex along the steep topography. To investigate the time evolution and the robustness of an initially isolated vortex analogous to the *LE anticyclone* (observed during the EGYPT campaign) we perform some numerical simulations with the Geostrophic Vorticity intermediate two-layer model (Sutyrin *et al.*, 2003). This intermediate model do not reproduce the dynamic of inertia-gravity waves and some agesotrophic instabilities. However, for a large-scale geostrophic vortex (i.e. small Rossby number) these fast component of motion should have a weak influence on the slow evolution of the eddy.

5.1 Scaling and derivation of intermediate equations

We consider a vortex with maximum velocity $V_m \approx 0.4\ m\ s^{-1}$ at the radius $R_m \approx 40\ km$. Choosing $f_0 \approx 8 \times 10^{-5}\ s^{-1}$, we find that the Rossby number, Ro, which

characterizes eddy strength relative to the planetary vorticity, is

$$Ro \equiv \frac{V_m}{f_0 R_m} \approx 0.15 \tag{29}$$

Given a typical reduced gravity $g' \approx 0.01$ ms^{-1}, a typical upper layer depth $h_0 \approx 150\ m$, and assuming the eddies are in geostrophic balance at leading order, we find that the ratio of the interface displacement to the upper layer depth,

$$\frac{f_0 V_m R_m}{g' h_0} \approx 1, \tag{30}$$

These nondimensional parameters indicate that the flow is essentially in geostrophic balance, but that depth variations in the upper layer can not be assumed small. This combination suggests an "intermediate" (between quasi-geostrophic and primitive) simplification of the momentum equations (3). Here we use an expansion in the Rossby number in the form first suggested by Sutyrin and Yushina (1986) and generalized for the multi-layer settings by Sutyrin et al. (2003). Under this approximation, the leading order flow is geostrophic,

$$v_g = \mathbf{k} \times \nabla p, \tag{31}$$

and the next order flow is expressed as

$$\mathbf{v} = \frac{1}{f + \zeta_g}(\mathbf{k} \times \nabla B - \nabla \partial_t p), \tag{32}$$

where $\zeta_g = \nabla^2 p$ is the geostrophic vorticity and $B = p + v_g^2/2$ is the geostrophic Bernoulli function. Inserting the expression (32) into the continuity equation (4) yields a predictive system of equations for p that involves only the geopotential field,

$$(-1)^j \partial_t h_1 + \nabla \cdot (PT_j \nabla \partial_t p_j) = J(B_j, PT_j) + (j-1) b \nabla^2 p_2, \tag{33}$$

where $PT = h/(f + \zeta_g)$ is the potential thickness (inverse potential vorticity) that is also conserved in fluid parcels moving with velocity described by (32). This

Geostrophic Vorticity intermediate model was shown to be the most accurate among the various forms of the General Geostrophic models that have been compared by Allen et al. (1990).

The vortex is initialized with a potential vorticity perturbation in the upper layer taking into account the image-effect to satisfy the boundary condition,

$$PT = \frac{P_\infty + Z(r) - Z(\tilde{r})}{f}, \tag{34}$$

$$Z(r) = A[1 - \tanh(-r^2)], \text{ and} \tag{35}$$

$$r = \frac{\sqrt{X^2 + Y^2}}{R_c}, \qquad \tilde{r} = \frac{\sqrt{x^2 + (Y + 2L)^2}}{R_c}, \tag{36}$$

where the vortex core parameters: $A = 2$ and $R_c = 3$ are chosen to initialize the upper layer vortex with negative vorticity at the center and maximum velocity $v_m \approx 0.3$ at the radius $r \approx 3$ (Figure 7). The initial velocity in the lower layer is zero.

The numerical scheme for Geostrophic Vorticity intermediate equation model uses a conservative Arakawa spatial approximation for the Jacobian on the right hand side of equation (33), and a second-order Adams-Bashforth approximation for each time step. The model domain is 40×27 with $\Delta x = \Delta y = 0.27$ grid resolution. Boundary conditions are no flux on the western, southern and northern boundaries, and the eastern boundary is open to allow topographic Rossby waves to propagate out of the domain. During calculations, the domain is shifted along-slope to keep the vortex in the center of the domain. Correspondingly, unperturbed conditions are prescribed at the western boundary.

5.2 Results of simulations

The slope in the lower layer was prescribed as $H' = S_0 + S_1 \exp(-\alpha(Y + L))$, where S_0 compensates the β-effect, so that $PT_2 \to const$ for large Y, while $S_1 = 2$ and $\alpha = 0.1$. This topographic profile is shown in Figure 8 together with the interface, the lower layer along-shore velocity and geopotential anomaly formed after the flow

is reached nearly steady-state. The velocity in the lower layer is mostly negative beneath the upper layer eddy resulting in amplification of its westward drift. The off-shore shift of the lower layer circulation is clearly seen in Figure 9 where the vortex center positions are compared with the reduced-gravity simulations. The deep anticyclone corresponds qualitatively to the analytic solution (23) and its feedback to the upper-layer vortex increases the drift speed by 85%. In dimensional units, the speed of the beta-drift is about 0.5 km/day while the image-effect adds 0.3 km/day in the reduced-gravity case, while the deep flow accelerates the vortex drift up to 1.5 km/day.

Note, it is steep topography that simplifies calculation of the vortex drift in comparison with a two-layer system on the beta-plane with flat bottom considered by Benilov (2000). When starting from a circular vortex in the upper layer, the initial development of a dipolar pattern due to stretching in the lower layer is quite similar. However, an eddy over flat bottom has westward component of translation resonating with Rossby waves, while over steep slope our eddy moves in equivalent eastward direction and reaches a steadily propagating stage described by our simple analytical solution.

6 Discussion and Conclusions

Motivated by the recent in-situ measurements of the EGYPT/EGGITO program, we have considered the effects of bathymetry on the propagation of intense, surface-intensified vortices on a β-plane in a two-layer model over non-uniformly sloping topography near the boundary. A perturbation theory is proposed for a circular vortex in the upper layer and the lower layer at rest as a basic state. The vortex propagation speed is found from the integral relations that describe the β-drift and image-effect in the reduced-gravity approximation, and an additional feedback due to

the lower-layer flow generated by vortex-stretching effects.

Without friction, a complete solution can be found only when all contours of the lower layer thickness are open. Most part of the lower-layer flow pattern can then be explained in terms of potential vorticity conservation. The stretching in the lower layer associated with β-induced and/or image-effect along-slope vortex interface migration should be balanced by a water advection generating by the deep flow pattern. The deep flow interacts with the upper layer according to the hydrostatic relation (5) and provides an additional along-slope vortex drift, which depends on the relative isopycnal displacement of the surface vortex λ, the vertical two-layer aspect ratio δ and the topographic slope parameter To. The asymptotic analysis shows that for steep shelves when $\delta \ll 1$, $To \gg 1$ and $\delta To \sim 1$ the deep flow feedback could double the along-slope drift velocity of the surface vortex. The stability of the steady drifting solution and the amplification of the along slope drift velocity were confirmed by numerical simulations having the same dynamical parameters than the *LE anticyclone*.

The instability of the Atlantic Water flow, namely the Libyo-Egyptian Current, generates anticyclones that are observed usually drifting eastward (Hamad *et al.* 2005, Millot and Taupier-Letage, 2005). However, we assume here that the *LE anticyclone* is isolated (no interaction with the background surface flow). In such case, the steep slope effect could explain its anomalously fast westward propagation along the Libyan shelf. We show here that a weak deep-flow feedback could significantly influence the drifting velocity of a stable surface vortex along a steep shelf.

Acknowledgements G.S. was funded by the NSF Division of Ocean Sciences and he greatly appreciates support and hospitality of the Laboratory of Dynamical Meteorology during his Visiting Professorship funded by the Ecole Normale Superieure and the Ecole Polytechnique. The authors thank P.M. Poulain and R.Gerin (OGS, Trieste, Italy) for making the drifters data of the joint EGITTO program available.

The EGYPT program received funding from INSU, LEFE/IDAO, GMMC/Mercator and the Regional Council Provence Alpes Ctes d'Azur. Thanks are extended to the ships crews.

References

Chassignet, E.P., Cushman-Roisin, B., 1991. On the influence of a lower-layer on the propagation of nonlinear oceanic eddies. *Journal of Physical Oceanography*, **21**, 939–957.

Benilov, E.S., 1996. Beta-induced transition of strong isolated eddies. *Journal of Physical Oceanography*, **26**, 2223–2229.

Benilov, E.S., 2000. The dynamics of a near-surface vortex in a two-layer ocean on the beta-plane. *J. Fluid Mech.*, **420**, 277–299.

Brown, O. B., P. C. Cornillon, S. R. Emmerson and H. M. Carle, 1986: Gulf Stream warm rings: a statistical study of their behavior. *Deep Sea Res.*, **33**, 1459–1473.

Carnevale, G. F., R. C. Kloosterziel and G. J. F. Van Heijst, 1991. Propagation of barotropic vortices over topography in a rotating tank. *J. Fluid Mech.*, **233**, 119–139.

Dewar, W.K., Leonov, D.A., 2004. Variability on Steep, Confined Topography. *Deep-Sea Res.* Part II, **51**, 2973–2993.

Evans, R.H., Baker, K.S., Brown, O.B., Smith, R.C., 1985. Chronology of warm-core ring 82B. *Journal of Geophysical Research*, **90**, 8803–8811.

Fratantoni, D.M., Johns, W.E., Townsend, T.L., 1995. Rings of the North Brazil Currents: Their structure and behavior inferred from observations and a numerical simulation. *Journal of Geophysical Research*, **100**, 10 663–10 654.

Firing, E. and R. C. Beardsley, 1976. The behavior of a barotropic eddy on a beta-plane. *J. Phys. Oceanogr.*, **6**, 57–65.

Freeland, H.J., Boland, F.M., Church, J.A., Clarke, A.J., Forbes, A.M.G., Huyer, A., Smith, R.L., Tompson, R.O.R.Y., White, N.J., 1986. The Australian Coastal Experiment: A search for coastal-trapped waves. *Journal of Physical Oceanography,* **16**, 1230–1249.

Frolov, S.A., Sutyrin, G.G., Rowe, G.D., Rothstein, L.M., 2004. Loop Current eddy interaction with the western boundary in the Gulf of Mexico. *Journal of Physical Oceanography*, **34**, 2223–2237.

Grimshaw, R., D. Broutman, Xinyu He and Pei Sun, 1994. Analytical and numerical study of a barotropic eddy on a topographic slope. *J. Phys. Oceanogr.*, **24**, 1587–1607.

Hamad, N., C. Millot and I. Taupier-Letage, 2005. A new hypothesis about the surface circulation in the eastern basin of the Mediterranean Sae. Prgr. In Oceanogr., **66**, 287-298.

Hamon, B., 1965. The East Australian Current 1960–1964. *Deep-Sea Research*, **12**, 899–921.

Jacob J.P., Chassignet, E.P., Dewar, W.K., 2002. Influence of topography on the propagation of isolated eddies. *Journal of Physical Oceanography,* **32**, 2848–2869.

Kamenkovich, V. M., Y. P. Leonov, D. A. Nechaev, D. A. Byrne and A. L. Gordon, 1996. On the influence of bottom topography on the Agulhas Eddy. *J. Phys. Oceanogr.*, **26**, 622–643.

Killworth, P.D., 1983. On the motion of isolated lenses on a β-plane. *Journal of Physical Oceanography*, **13**, 368–376.

Kirwan, A. D. Jr., Lewis, J.K., Indest, A.W., Reinersman, P., Quintero, I., 1988. Observed and simulated kinematic properties of Loop Current rings. *Journal of Geophysical Research*, **93**, 1189–1198.

Kizner Z., G. Reznik, D. Berson, and G.G. Sutyrin, 2003. The theory of the

beta-plane baroclinic topographic modons. *Geophys. Astrophys. Fluid Dyn.*, **97**, 175–211.

Lingevitch, J.P. Bernoff, A.J., 1994. Advection of a passive scalar by a vortex couple in the small-diffusion limit. *Journal of Fluid Mechanics*, **270**, 219–249.

Louis, J. P. and P. S. Smith, 1982. The development of the barotropic radiation field of an eddy on a slope. *J. Phys. Oceanogr.*, **12**, 56–73.

Masuda, A. Marubayashi, K. & Ishibashi, M. 1990. A laboratory experiment and numerical simulation of an isolated barotropic eddy with topographic β. *J. Fluid Mech.*, **213**, 641-659.

McDonald, N. R., 1998. The motion of an intense vortex near topography. *J. Fluid Mech.*, **367**, 359–377.

Millot, C. and I. Taupier-Letage, 2005. Circulation in the Mediterranean Sea. The Handbook of Environmental Chemistry, Volume 5 Part K Alain Saliot volume Ed., Springer-Verlag, 29-66. DOI: 10.1007/b107143.

Nezlin, M.V., Sutyrin, G.G., 1994. Problems of simulation of large, long-lived vortices in the atmospheres of the giant planets (Jupiter, Saturn, Neptune). *Surveys in Geophysics,* **15**, 63–99.

Nof, D., 1983. On the migration of isolated eddies with application to Gulf Stream Rings. *Journal of marine Research*, **1**, 399–425.

Puillat I., I. Taupier-Letage and C. Millot, 2002. Algerian eddies lifetimes can be near 3 years. *Journal of marine Syst.*, **31**, 4: 245-259.

Reznik G.M., and G.G. Sutyrin, 2001. Baroclinic topographic modons. *J. Fluid Mech.*, **437**, 121–142.

Richardson, G., 2000. Vortex motion in shallow-water with varying bottom topography and zero Froude-number. *J. Fluid Mech.*, **411**, 351–374.

Smith, D. C. IV., 1986. A numerical study of Loop Current eddy interaction with

topography in the western Gulf of Mexico. *J. Phys. Oceanogr.*, **16**, 1260–1272.

Smith, D. C. IV and J. J. O'Brien, 1983. The interaction of a two-layer isolated mesoscale eddy with bottom topography. *J. Phys. Oceanogr.*, **13**, 1681–1697.

Stegner, A. and Zeitlin, V., 1995. What can asymptotic expansions tell us about large-scale quasi-geostrophic anticyclonic vortices? *Nonlinear Processs in Geophysics*, **2**, 186–193.

Stegner, A. and Zeitlin, V., 1996. Asymptotic expansions and monopolar solitary Rossby vortices in barotropic and two-layer models. *Geophysical and Astrophysical Fluid Dynamics*, **83**, 159–195.

Sutyrin, G.G., 2001. Effects of topography on the β-drift of a baroclinic vortex. *Journal of marine Research,* **59**, 977–989.

Sutyrin, G.G., Grimshaw, R., 2005. Frictional effects on the deep-flow feedback on the β-drift of a baroclinic vortex over sloping topography. *Deep Sea Res., Part I*, **52**, 2156–2167.

Sutyrin, G., Rowe, D., Rothstein, L., Ginis, I., 2003. Baroclinic-eddy interactions with continental slopes and shelves. *Journal of Physical Oceanography,* **33**, 283–291.

Taupier Letage, I. 2008. On the use of thermal infrared images for circulation studies: applications to the eastern Mediterranean basin. In "Remote sensing of the European Seas" V. Barale and M. Gade Eds., Springer Verlag, 153-164.

Thierry, V., Morel, Y., 1999. Influence of a strong bottom slope on the evolution of a surface-intensified vortex. *Journal of Physical Oceanography,* **29**, 911–924.

Thompson, L., 1993. Two-layer quasigeostrophic flow over finite isolated topography. *J. Phys. Oceanogr.*, **23**, 1297–1314.

Van Geffen J. H. G. M. and P. A. Davies, 1999. Interaction of a monopolar vortex with a topographic ridge. *Geophys. Astrophys. Fluid Dyn.*, **90**, 1–41.

Van Heijst, G. J. F., 1994. Topography effects on vortices in a rotating fluid.

Mecanica, **29**, 431–451.

Umatani, S. and T. Yamagata, 1987. Evolution of an isolated eddy near a coast and its relevance to the "Kyucho." *J. Ocean. Soc. Japan*, **43**, 197–203.

Vukovich, F. M., Waddell, E., 1991. Interaction of a warm ring with the western slope in the Gulf of Mexico. *Journal of Physical Oceanography,* **21,** 1062–1074.

Wang, X., 1992. Interaction of an eddy with a continental slope. Ph.D. thesis, MIT/WHOI Joint Proram in Oceanography, 216 pp.

White, A.J., McDonald, N.R., 2004. The motion of a point vortex near large-amplitude topography in a two-layer fluid. *J. Phys. Oceanogr.* **34**, 2808–2824.

Zavala Sanson, L., van Heijst, G.J.F., 2002. Ekman effects in a rotating flow over bottom topography. *Journal of Fluid Mechanics*, **471**, 239–255.

$Ro = \frac{V_0}{fR}$	$Bu = \left(\frac{R_d}{R}\right)^2$	$\lambda = \frac{\Delta h}{h_0}$	$\alpha = h_0/R$	$\delta = \frac{h_0}{H_0}$	$C = \frac{V_{LE}}{V_0}$	$To = \frac{s}{\alpha}$
$0.1 - 0.15$	$0.14 - 0.18$	~ 1	~ 0.005	~ 0.08	$0.03 - 0.06$	~ 20

Table I Dimensionless parameters of the meso-scale *LE anticyclone*.

Figure Captions

Figure 1 Surface drifter trajectories of buoys B557312 (a), B59774 (b) and B59777 (c) trapped within the core of a large scale Libyo-Egyptian anticyclone (*LE* anticyclone). The mean eddy trajectory from april to september 2006 is plotted in (d). The dots in (d) correspond to the vertical CTD profiles taken from april 19 to april 21.

Figure 2 Instantaneous buoys velocities as a function of the radial distance to the vortex center.

Figure 3 Vertical density cross section of the *LE* anticyclone along the seafloor bathymetry (a). Isopycnal devations of the *LE* anticyclone close to the steep shelf slope (b).

Figure 4 Two-layers modelisation of a surface intensified anticyclone along a steep shelf bathymetry.

Figure 5 Upper layer (a) and lower layer (b) streamlines in the steady drifting frame for a gaussian vortex having similar parameters than the *LE* anticyclone: $c = 0.7$, $\delta = 0.08$, $To = 20$ and $L = 2$.

Figure 6 Evolution of the acceleration coefficient γ as a function of the product δTo (for various values of $\delta = 0.06, 0.08, 0.1$) (a) and as a function of the relative isopycnal deviation parameter λ (b).

Figure 7 Initial along-shore velocity and vorticity (dashed) across the vortex.

Figure 8 The csross-isobath profiles of the ocean depth (thick line), the upper layer interface (dashed), the lower layer geopotential (thin line) and corresponding along-shore velocity (dotted) after 6 months of integration.

Figure 9 The vortex center positions each 10 days for 6 months (circles) to compare with the reduced-gravity simulations (dots) for the same distance from the wall $L = 4.3$. Contours of interface and the lower layer pressure (dashed lines) are plotted at the final time when the solution is nearly stationary.

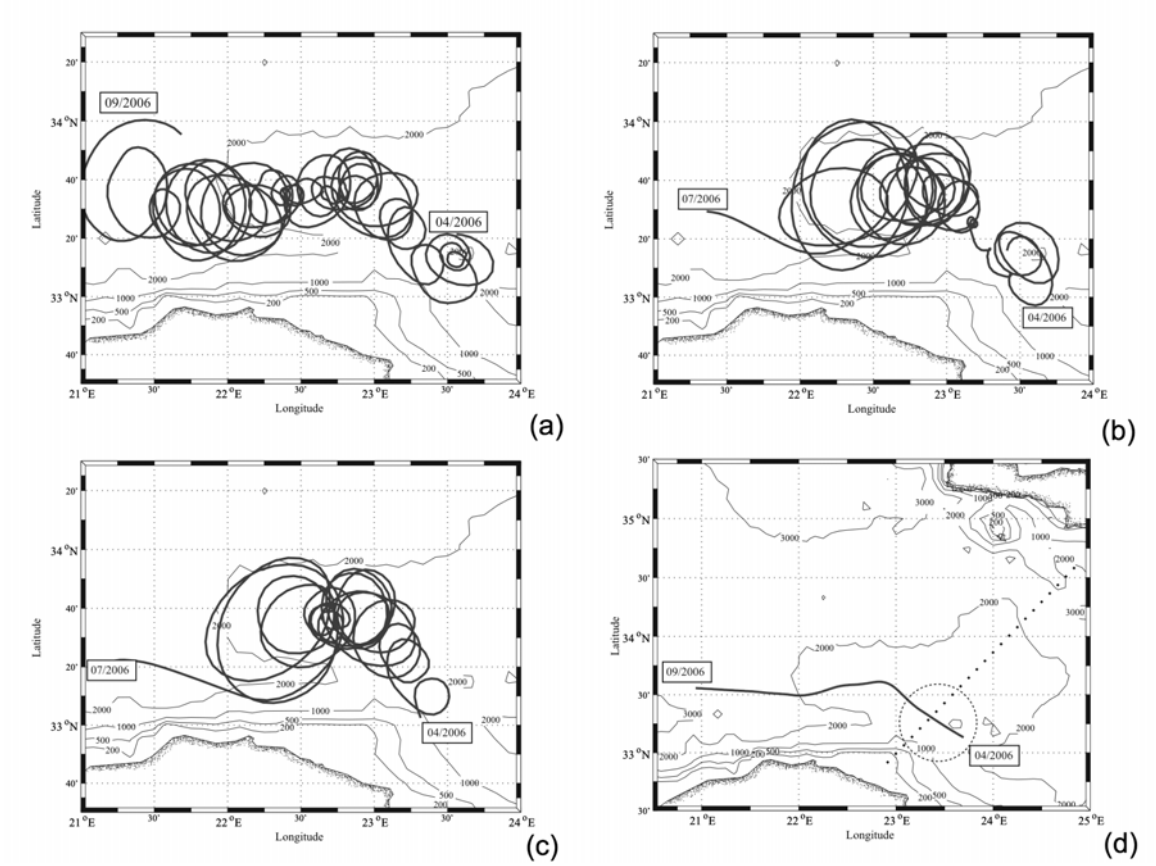

Figure 1. Surface drifter trajectories of buoys B557312 (a), B59774 (b) and B59777 (c) trapped within the core of a large scale Libyo-Egyptian anticyclone (LE anticyclone). The mean eddy trajectory from April to September 2006 is plotted in (d). The dots in (d) correspond to the vertical CTD profiles taken from April 19 to April 21.

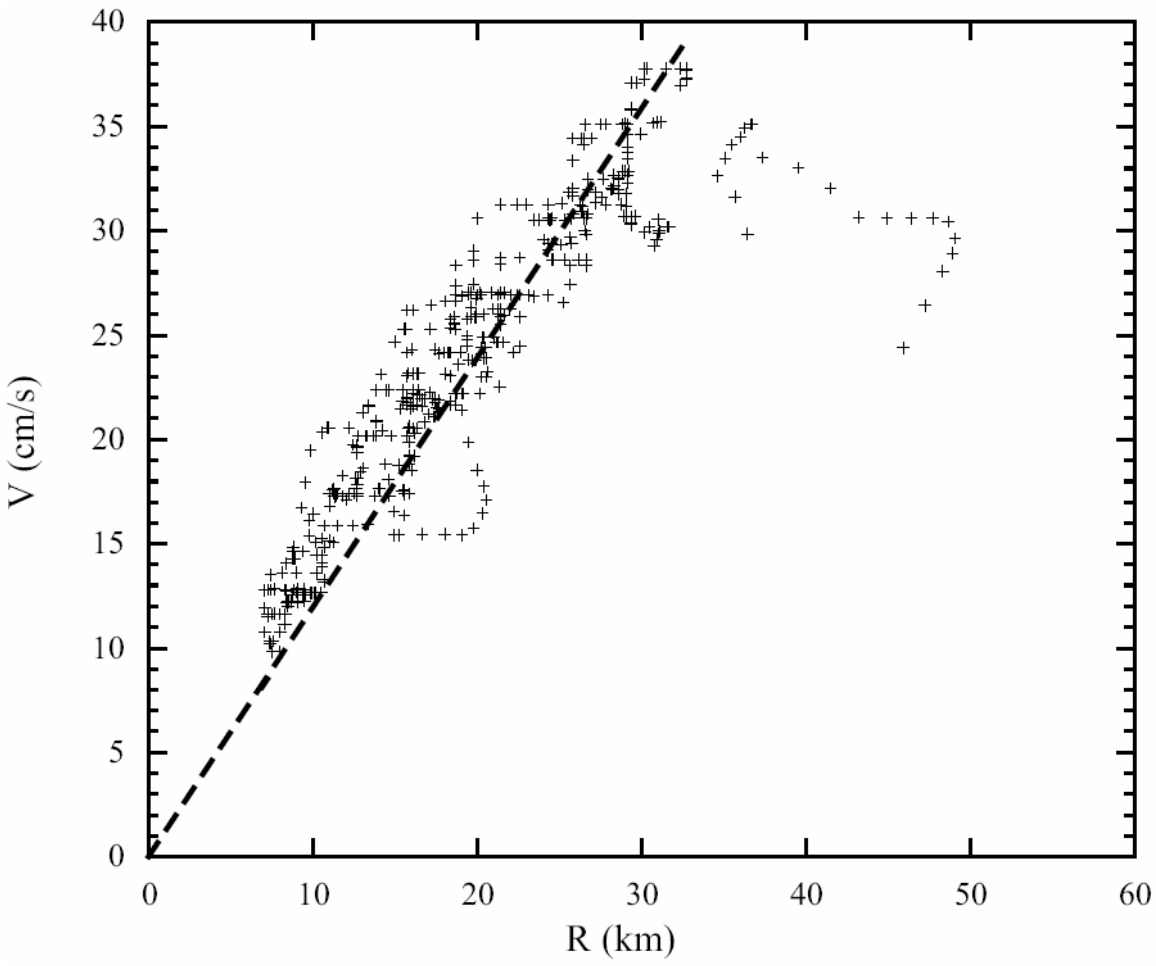

Figure 2. Instantaneous buoys velocities as a function of the radial distance to the vortex center.

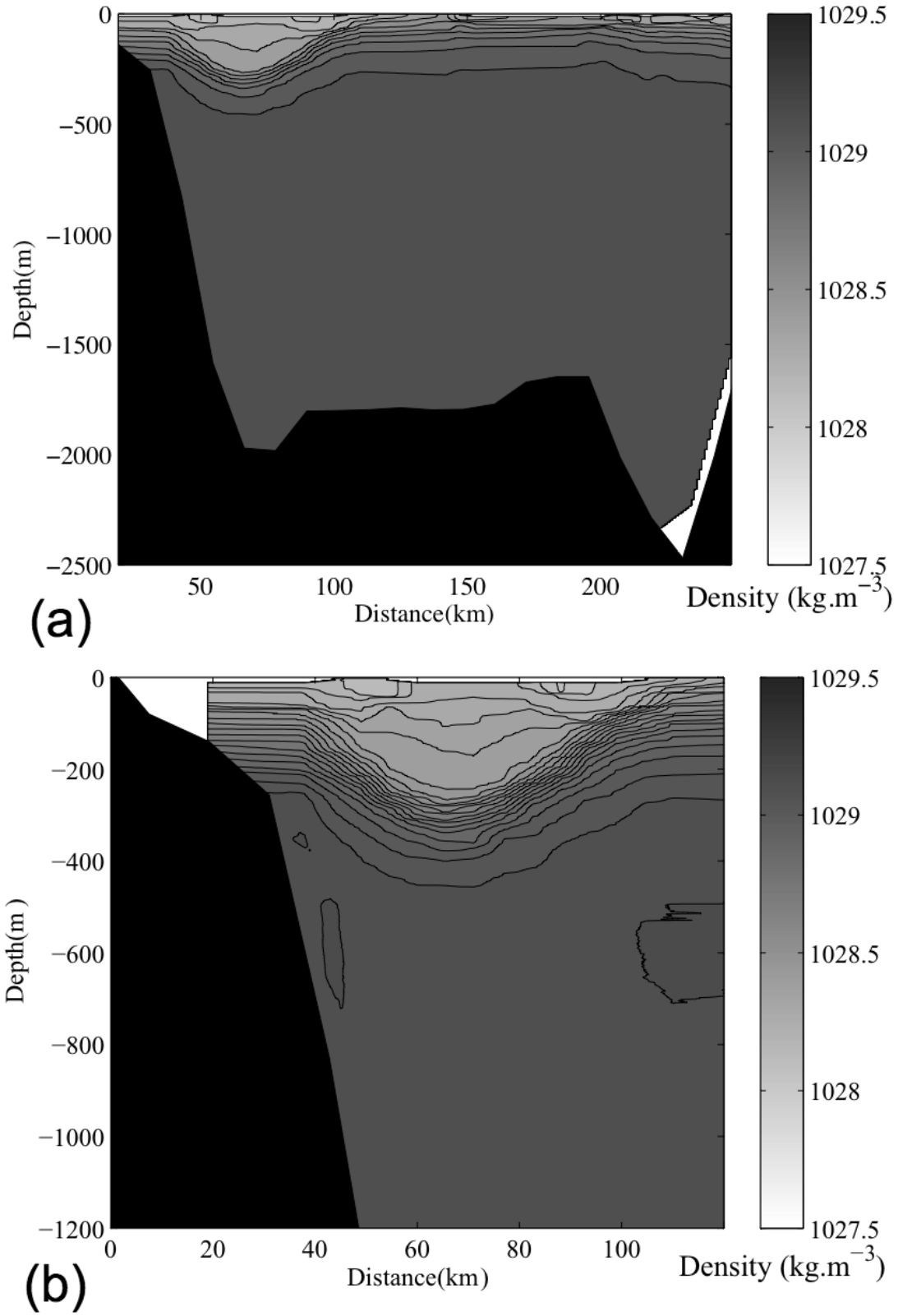

Figure 3. Vertical density cross section of the LE anticyclone along the seafloor bathymetry (a). Isopycnal devations of the LE anticyclone close to the steep shelf slope (b).

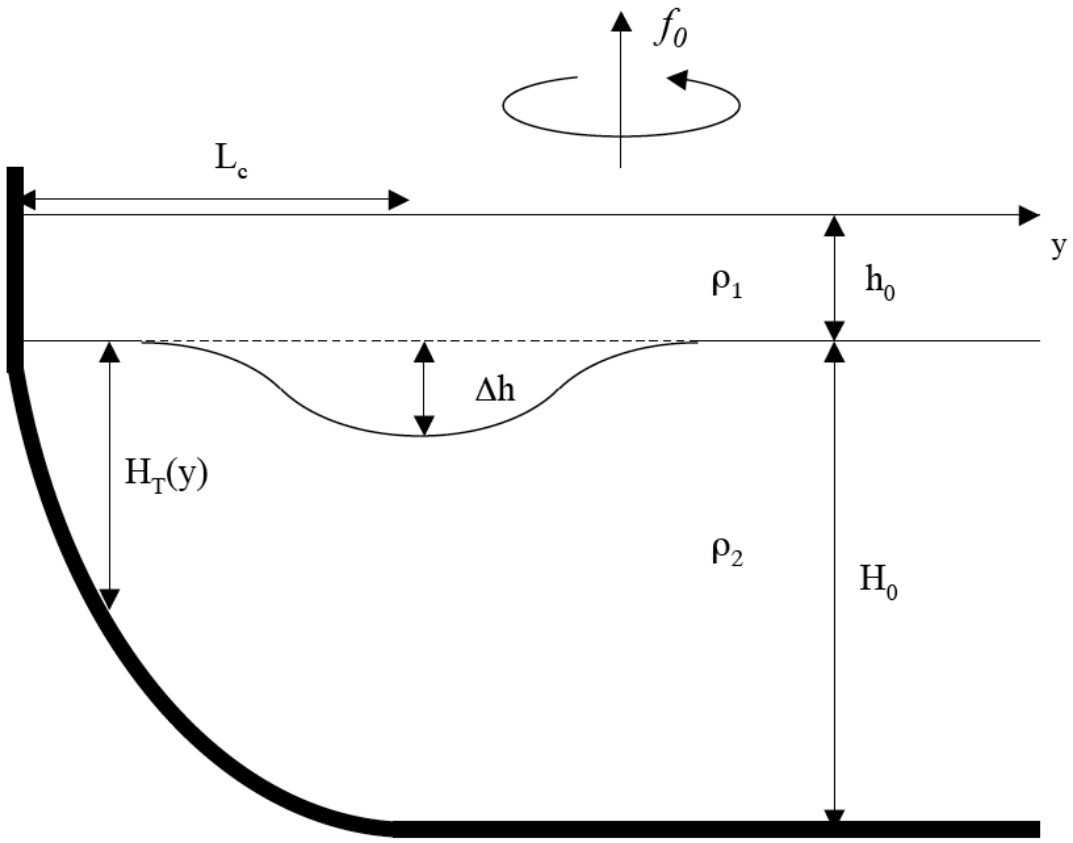

Figure 4. Two-layer schematic of a surface intensified anticyclone along a steep shelf bathymetry.

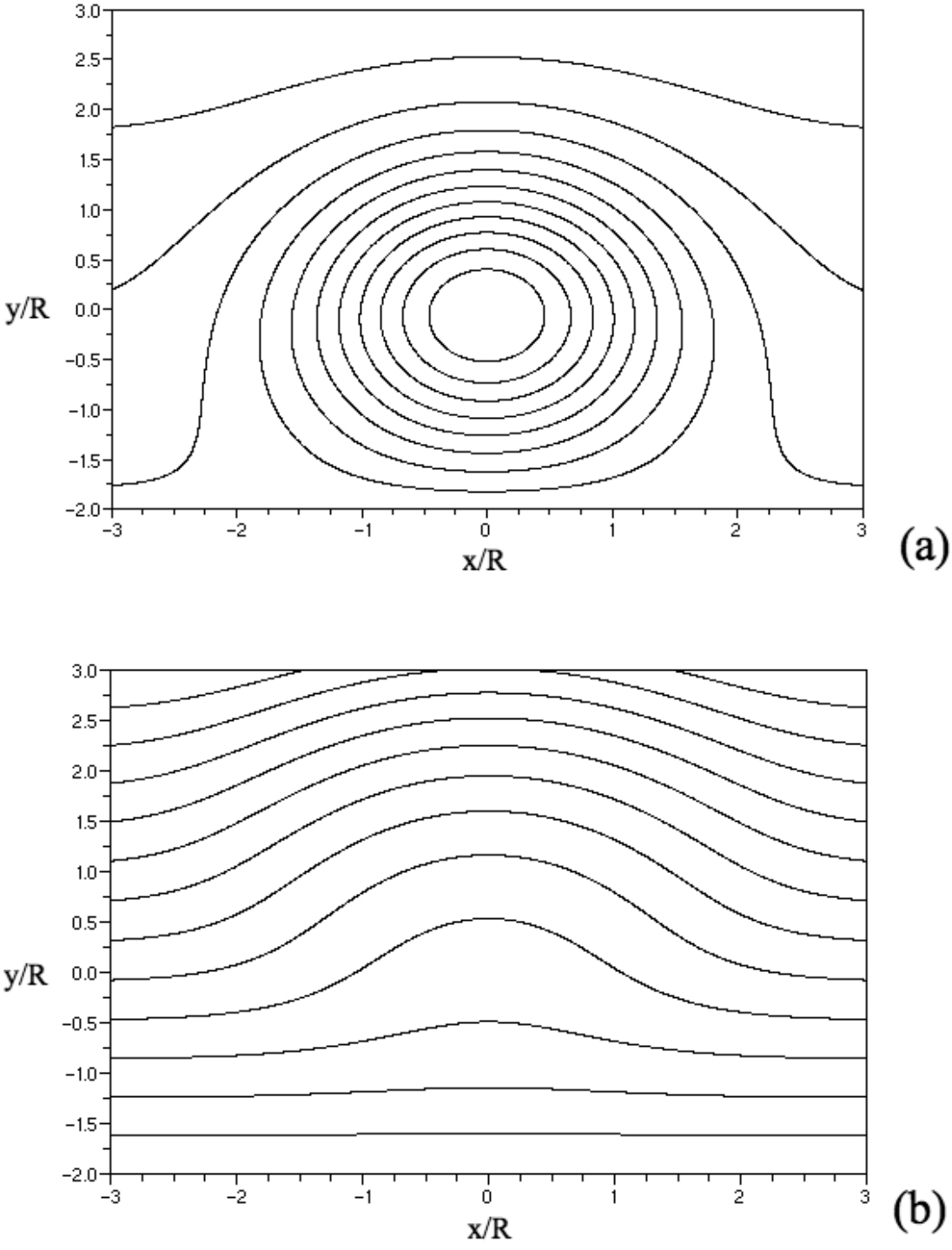

Figure 5. Upper layer (a) and lower layer (b) streamlines in the steady drifting frame for a Gaussian vortex having parameters similar to the LE anticyclone: $c = 0.7$, $\delta = 0.08$, $To = 20$ and $L = 2$.

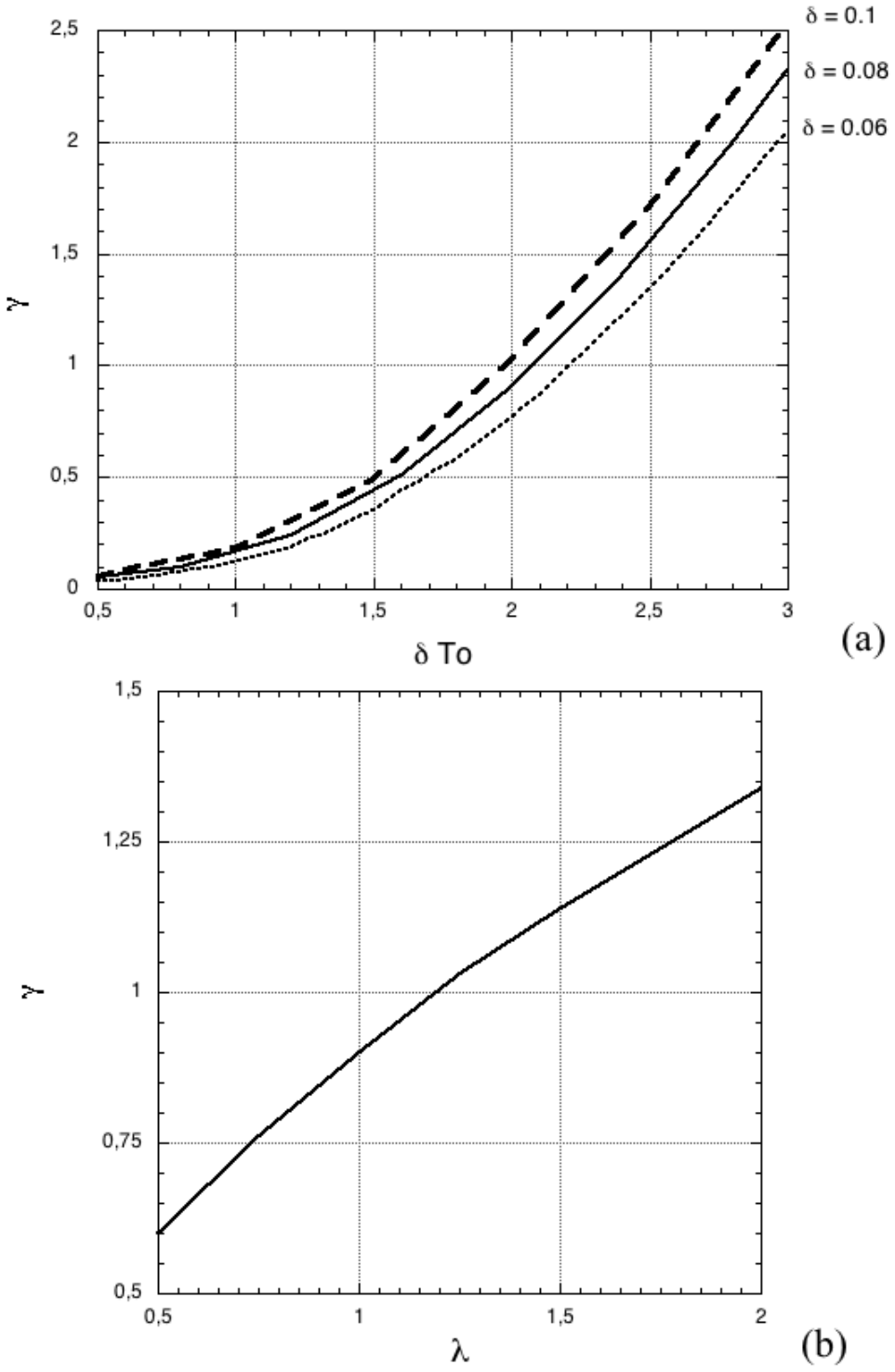

Figure 6. Evolution of the acceleration coefficient γ as a function of the product δTo (for various values of δ = 0.06; 0.08; 0.1) (a) and as a function of the relative isopycnal deviation parameter λ (b).

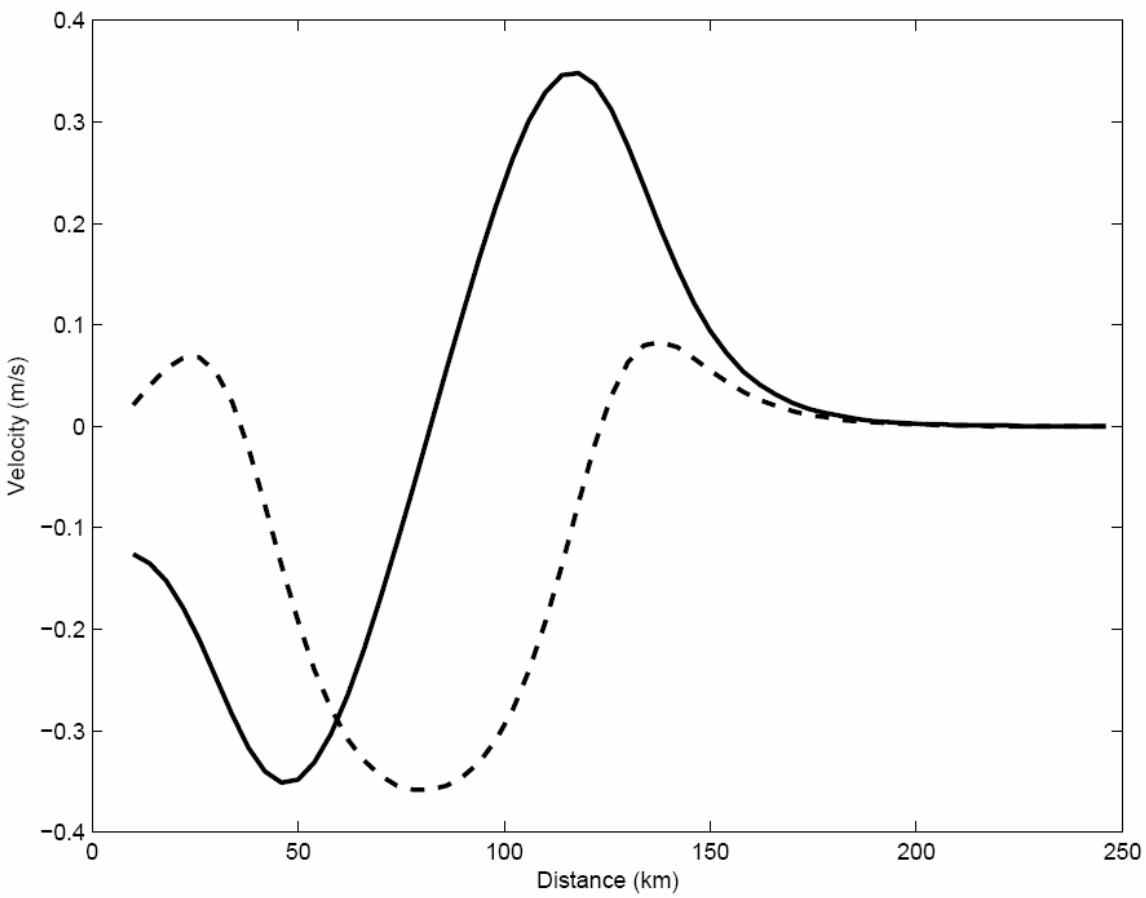

Figure 7. Initial along-shore velocity and vorticity (dashed) across the vortex.

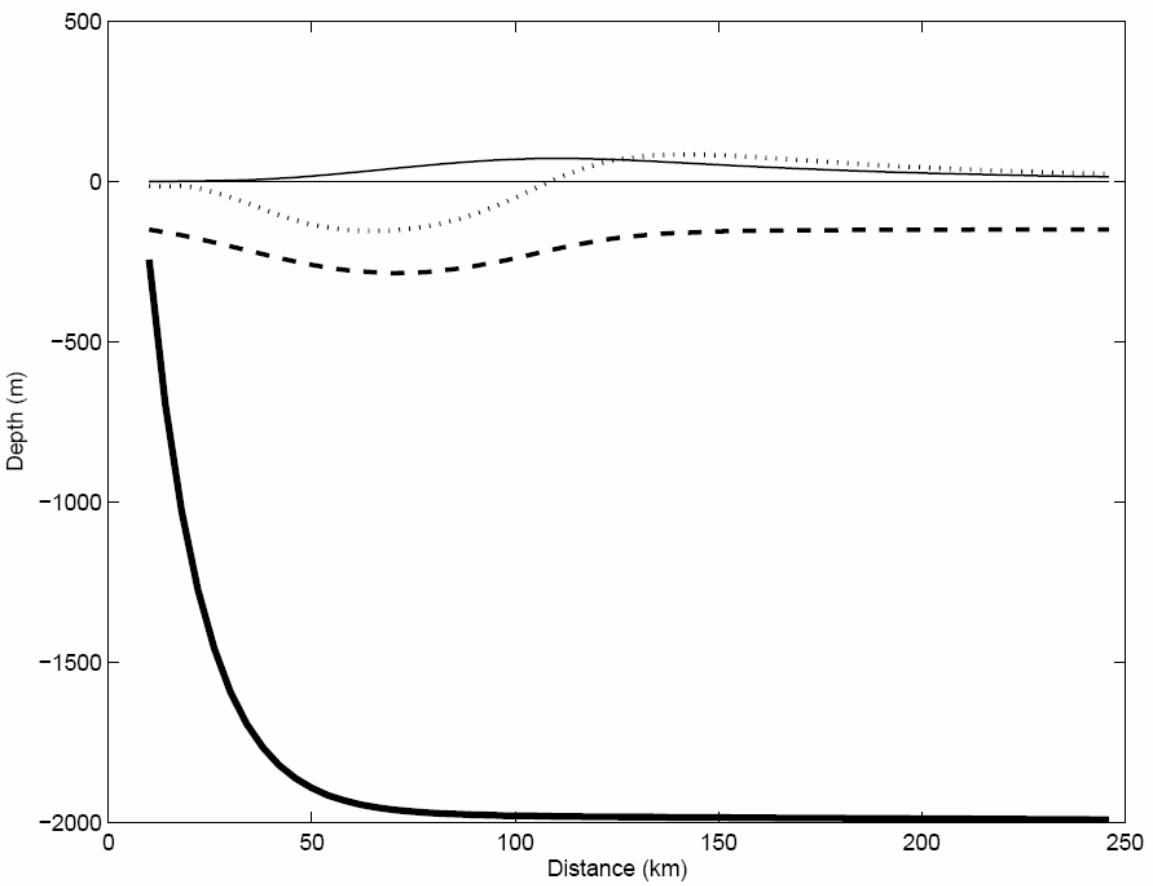

Figure 8. The csross-isobath profiles of the ocean depth (thick line), the upper layer interface (dashed), the lower layer geopotential (thin line) and corresponding along-shore velocity (dotted) after 6 months of integration.

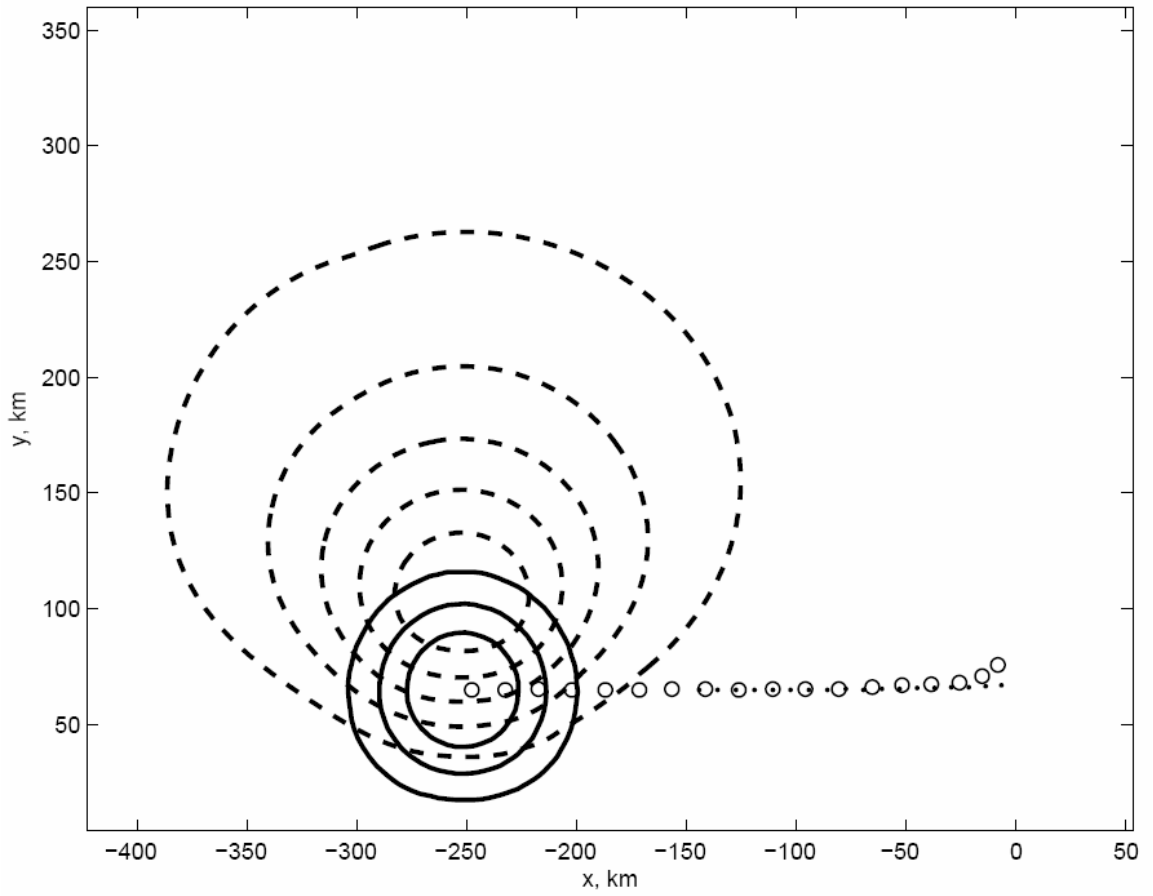

Figure 9. The vortex center positions each 10 days for 6 months (circles) to compare with the reduced-gravity simulations (dots) for the same distance from the wall L = 4.3. Contours of interface and the lower layer pressure (dashed lines) are plotted at the final time when the solution is nearly stationary.